Biochemical Journal (2023) **480** 1411–1427
https://doi.org/10.1042/BCJ20230207

PORTLAND PRESS

Research Article

Cancer-associated somatic mutations in human phosphofructokinase-1 reveal a critical electrostatic interaction for allosteric regulation of enzyme activity

Maria A. Voronkova[1], Heather L. Hansen[1], Madison P. Cooper[1], Jacob Miller[1], Narayanasami Sukumar[2], Werner J. Geldenhuys[3], Aaron R. Robart[1] and Bradley A. Webb[1]

[1]Department of Biochemistry, West Virginia University School of Medicine, Morgantown, WV 26506, U.S.A.; [2]Northeastern Collaborative Access Team Center for Advanced Macromolecular Crystallography, Argonne National Laboratory, Lemont, IL 60439, U.S.A.; [3]Department of Pharmaceutical Sciences, West Virginia University School of Pharmacy, Morgantown, WV 26506, U.S.A.

Correspondence: Bradley A. Webb (bradley.webb@hsc.wvu.edu)

OPEN ACCESS

Metabolic reprogramming, including increased glucose uptake and lactic acid excretion, is a hallmark of cancer. The glycolytic 'gatekeeper' enzyme phosphofructokinase-1 (PFK1), which catalyzes the step committing glucose to breakdown, is dysregulated in cancers. While altered PFK1 activity and expression in tumors have been demonstrated, little is known about the effects of cancer-associated somatic mutations. Somatic mutations in PFK1 inform our understanding of allosteric regulation by identifying key amino acid residues involved in the regulation of enzyme activity. Here, we characterized mutations disrupting an evolutionarily conserved salt bridge between aspartic acid and arginine in human platelet (PFKP) and liver (PFKL) isoforms. Using purified recombinant proteins, we showed that disruption of the Asp–Arg pair in two PFK1 isoforms decreased enzyme activity and altered allosteric regulation. We determined the crystal structure of PFK1 to 3.6 Å resolution and used molecular dynamic simulations to understand molecular mechanisms of altered allosteric regulation. We showed that PFKP-D564N had a decreased total system energy and changes in the electrostatic surface potential of the effector site. Cells expressing PFKP-D564N demonstrated a decreased rate of glycolysis, while their ability to induce glycolytic flux under conditions of low cellular energy was enhanced compared with cells expressing wild-type PFKP. Taken together, these results suggest that mutations in Arg–Asp pair at the interface of the catalytic-regulatory domains stabilizes the *t*-state and presents novel mechanistic insight for therapeutic development in cancer.

Introduction

Glycolysis is an ancient pathway that breaks down glucose to generate energy, reducing agents, and biosynthetic precursors to support cellular functions. Adenosine triphosphate (ATP) produced by the glycolytic pathway is a major source of energy for cellular activities including muscle contraction, the transmission of neuronal signals, and active transport. In addition to ATP, glycolysis generates metabolic intermediates that serve as anabolic building blocks for cellular components such as DNA, lipids, and proteins. While glycolysis is essential for normal cell function, its dysregulation has been linked to the initiation and progression of many diseases, including cancer, diabetes, and neurodegenerative disorders. Aberrant activation of glycolysis can promote tumor growth and metastasis by providing cancer cells with energy and metabolic intermediates necessary for their survival [1]. Similarly,

Received: 29 May 2023
Revised: 23 August 2023
Accepted: 25 August 2023

Accepted Manuscript online: 25 August 2023
Version of Record published: 4 September 2023

Biochemical Journal (2023) **480** 1411–1427
https://doi.org/10.1042/BCJ20230207

dysregulated glycolysis in diabetes can lead to the accumulation of toxic byproducts that damage tissues and impair insulin sensitivity [2]. In neurodegenerative diseases such as Alzheimer's, disrupted glucose metabolism has been shown to impair neuronal function and contribute to disease progression [3]. Therefore, determining the molecular mechanisms underlaying aberrant glycolysis in disease initiation and progression is essential for developing novel therapeutic interventions.

The rate of glycolytic flux is determined largely by the activity of rate-limiting enzymes, one of the most important of which is phosphofructokinase-1 (PFK1). PFK1 is known as the 'gatekeeper' of glycolysis catalyzing the reaction committing glucose to breakdown by irreversibly converting fructose 6-phosphate (F6P) to fructose 1,6-bisphosphate (F1,6bP). PFK1 is highly evolutionarily conserved, from bacteria to humans. Prokaryotic PFK1 protomers are approximately half the size of their mammalian counterparts and are less allosterically regulated [4,5]. Eukaryotic PFK1 evolved from a prokaryotic ancestral enzyme by gene duplication, tandem fusion, and evolution which created a novel tetramer interface, an amino-terminal 'catalytic' domain, and a carboxy-terminal 'regulatory' domain (Figure 1A,B) [6–8]. The increased size and complexity of eukaryotic PFK1 enabled enhanced allosteric regulation, with catalytic activity tightly controlled through multiple mechanisms including allosteric regulation by small molecule effectors, post-translational modification, and modulation of protein levels through transcriptional and post-translational mechanisms [9–13]. In general, signals of low cellular energy activate enzymatic activity while signals of high energy inhibit PFK1. PFK1 is inactive as individual or dimers of protomers but active as tetramers [14]. The shift between active tetramers and inactive protomers is regulated by small molecule effectors, with inhibitors promoting tetramer disassembly and activators promoting tetramer assembly [14–17].

Three PFK1 gene products exist in mammalian cells: muscle (PFKM), liver (PFKL), and platelet (PFKP). All three gene products are present at various levels in most tissues, except for skeletal muscle, which almost exclusively expresses PFKM, and the liver which predominantly expresses PFKL [18,19]. PFK1 can form homo- and hetero-tetramers, with some isoforms being able to assemble into larger catalytically active structures [20–22]. The genes encoding these isozymes are located on different chromosomes, with alternative splicing resulting in several transcript isoforms for each gene. The three human PFK1 isoforms are ∼70% identical at the amino acid level, with the differences in sequence accounting for isoform-specific regulation and activity. For instance, PFKM has the highest affinity for F6P and displays pH-dependent ATP inhibition while PFKP has greater activation by ADP/AMP and the highest level of inhibition by citrate [7,23,24]. The binding of biphosporylated hexoses, specifically fructose 1,6-bisphosphate (F1,6bP) and fructose 2,6-bisphosphate (F2,6bP), also has isoform-specific effects on PFK1. F2,6bP is the most potent natural agonist of PFK1; it both stabilizes and relieves ATP inhibition in all three human PFK1 isoforms. PFKP and PFKL show increased sensitivity to F2,6bP allosteric modulation compared with PFKM. Conversely, F1,6bP stabilizes all three human PFK1 isoforms but only relieves ATP inhibition in PFKL and PFKM [25–27].

Dysregulation and mutations of PFK1 have been implicated in the initiation and progression of various human diseases. For example, somatic missense and frameshift mutations in PFKM can cause glycogen storage disease type VII (Tarui disease), an autosomal recessive disease that impairs glycogen breakdown [28,29]. It is unclear whether somatic mutations in PFK1 contribute to other diseases such as cancer. Many cancer cells exhibit elevated glucose uptake and lactic acid excretion regardless of oxygen levels, a phenomenon known as the Warburg effect [30,31]. This altered metabolic program supplies energy and building blocks required to sustain rapid proliferation and adaption to the tumor microenvironment. Consistent with increased glycolytic flux, PFK1 expression and activity are elevated in cancer cell lines and primary tumors [32,33]. However, recent findings have demonstrated that metabolic reprogramming of cancer cells is more complex, suggesting that metabolic flexibility is essential for cancer initiation and progression [34–36]. In line with this idea, post-translational modifications which inhibit or degrade PFK1, such as glycosylation and ubiquitination, are also increased in cancers [10,11,37]. Hundreds of cancer-associated somatic mutations have been identified between the three human PFK1 genes. However, the impact of these mutations and their contribution to disease initiation and progression is unknown. While most disease-associated mutations in PFK1 are thought to inactivate the enzyme in a recessive manner, such as those identified in Tarui disease, we previously identified a cancer-associated mutation in PFK1, PFKP-D564N, that acted in a dominant manner when expressed in cells [15]. In this study, we characterized how cancer-associated somatic mutations of this critical aspartic acid-arginine pair alter the biochemical and structural regulation of PFK1, providing insights into the molecular mechanisms underlying allosteric regulation of human PFK1.

Biochemical Journal (2023) **480** 1411–1427
https://doi.org/10.1042/BCJ20230207

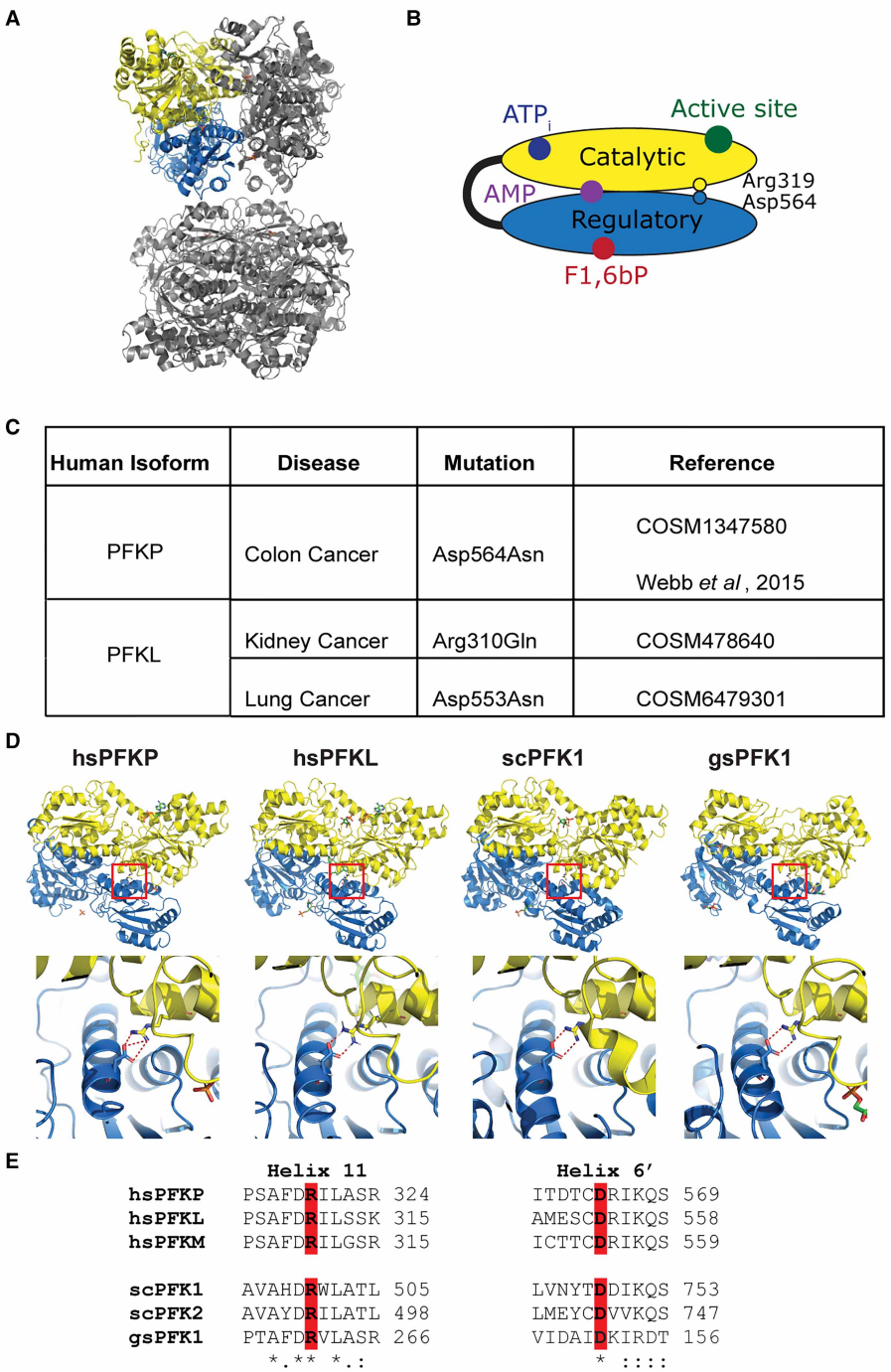

Human Isoform	Disease	Mutation	Reference
PFKP	Colon Cancer	Asp564Asn	COSM1347580 Webb *et al* , 2015
PFKL	Kidney Cancer	Arg310Gln	COSM478640
	Lung Cancer	Asp553Asn	COSM6479301

Figure 1. Arg319 and Asp564 are evolutionarily conserved. Part 1 of 2

(**A**) A ribbon diagram of the PFKP tetramer with the catalytic (yellow) and regulatory (blue) domain shown on one protomer. (**B**) Schematic of the catalytic and regulatory domains of a human PFK1 protomer viewed from the catalytic interface. The location of arginine 319 and aspartic acid 564 as well as effector-binding sites are labeled. (**C**) Cancer-associated somatic mutations to the Arg–Asp pair in human PFK1 isoforms from the COSMIC database [68]. (**D**) Low and high magnification views of residues orthologous to arginine 319 and aspartic acid 564 are shown on the structures of *Homo sapiens* PFKP (4XYK), *Homo sapiens* PFKL (7LW1), *Saccharomyces cerevisiae* PFK1 (3O8O), and *Geobacillus stearothermophilus* PFK1 (6PFK). The catalytic interface is orientated out of the page. For eukaryotic structures, a single protomer is shown, with the tetramer interface is oriented to the bottom and the catalytic site to the top. For the prokaryotic structure, a dimer of protomers is shown (blue and yellow), with the catalytic sites oriented to the top and bottom of the image. Predicted electrostatic interactions are represented

Biochemical Journal (2023) **480** 1411–1427
https://doi.org/10.1042/BCJ20230207

Figure 1. Arg319 and Asp564 are evolutionarily conserved. Part 2 of 2

by red dots. (**E**) Sequence alignment of human PFKP, PFKL, PFKM, *S. cerevisiae* PFK1 and PFK2, and *G. stearothermophilus* PFK1. Arginine 319 and aspartic acid 564 are highlighted in red.

Results

Evolutionarily conserved Asp–Arg pair is mutated in cancers

Aspartic acid 564 is located near the catalytic interface of human PFKP on helix 6′ (*E. coli* numbering) [38]. The carboxylic acid group of aspartic acid 564 faces the guanidine group of arginine 319 on helix 11 and the pair was predicted to form an electrostatic interaction. Somatic mutations to either the aspartic acid or arginine were found in multiple PFK1 isoforms (Figure 1C). In PFKL, mutations to both the homologous aspartic acid and arginine residues were identified, where aspartic acid 553 was changed to asparagine in kidney cancer and the arginine was replaced with a glutamine in lung cancer. While PFKM did not have mutation to the orthologous residues, mutations in adjacent residues, aspartic acid 309 and arginine 555, have been reported in Tarui disease and cancers, respectively [39].

We asked if the Asp–Arg pair was evolutionarily conserved by performing sequence and structural alignments. We found that residues homologous to Arg319 and Asp564 were conserved in single-cell eukaryotes such as *Saccharomyces cerevisiae* and in prokaryotes such as *Geobacillus stearothermophilus* PFK1 (Figure 1D,E and Supplemental Table S1). *S. cerevisiae* has two PFK1 subunits, PFK1 and PFK2, which form a hetero octamer. The octamer is a dimer of tetramers, with each tetramer equivalent in size and shape to the mammalian PFK1 tetramer. Both PFK1 and PFK2 subunits have residues orthologous to arginine 319 and aspartic acid 564 and are predicted to form an electrostatic interaction. PFK1 from prokaryotes is half the size of their eukaryotic orthologs, with the prokaryotic dimer equivalent in size to the eukaryotic protomer. Using PFK1 from *G. stearothermophilus* as a representative structure of bacterial PFK1, we found that the arginine and aspartic acid residues are conserved and located at the dimer interface, with the arginine from one protomer interacting with the aspartic acid from a second protomer. In summary, the location of aspartic acid 564 and an electrostatic interaction with arginine 319 are evolutionarily conserved from bacteria to humans, suggesting an important role in PFK1 activity.

Disruption of the Asp–Arg pair alters PFK1 activity and regulation

We generated recombinant human protein to determine the impact of cancer-associated mutations on PFK1 structure, activity, and regulation. Wild-type and mutant PFK1 proteins were expressed in a baculovirus expression system and purified to homogeneity, as determined by Coomassie-stained SDS–PAGE gels (Supplemental Figure S1). While we successfully generated PFKP-D564N and PFKL-D553N, we were unable to express and purify PFKL-R310Q, and therefore PFKL-R310Q was excluded from further analysis. We hypothesize that the less conservative nature of the arginine to glutamine substitution decreased the stability of the mutant protein. Native-PAGE analysis of purified protein was performed to determine if the mutations dramatically altered the quaternary structure of the enzyme. PFK1 protomers are ∼90 kDa in size, but assemble into tetramers of ∼480 kDa, as shown by Native-PAGE (Supplemental Figure S1). Bands larger than tetramers were also observed, predominantly in lanes containing PFKL, consistent with the ability of PFKL to form filaments of stacked tetramers [20]. No significant differences were observed between the wild-type and mutant PFK1 proteins, suggesting that the mutations do not alter the assembly of PFK1 into tetramers.

Next, we asked if a disruption of the Asp–Arg pair altered enzyme activity or allosteric regulation of PFKP. Consistent with our previous findings [15], recombinant PFKP-D564N had decreased maximum velocity of reaction, decreased affinity for the substrate fructose 6-phosphate (F6P), and decreased cooperativity when compared with wild-type PFKP (Figure 2A and Table 1). We tested if the mutation altered the allosteric regulation of three effectors. First, we examined the response to ATP, which is both a substrate and allosteric inhibitor of PFK1. The amino-terminal catalytic domain of eukaryotic PFK1 contains an inhibitory ATP binding site with mM affinity [8,40]. Under the conditions tested, both wild-type and mutant PFKP showed similar inhibition by ATP, with ∼50% inhibition observed at 4 mM (Figure 2B). This suggests that disruption of the Asp–Arg electrostatic interaction at the domain interface does not significantly affect allosteric regulation by ATP. Next, we asked if activation by adenosine monophosphate (AMP), a signal of low cellular energy, was altered. AMP/ADP binds with high μM affinity to its effector-binding site located in the center of the PFK1 protomer

Biochemical Journal (2023) **480** 1411–1427
https://doi.org/10.1042/BCJ20230207

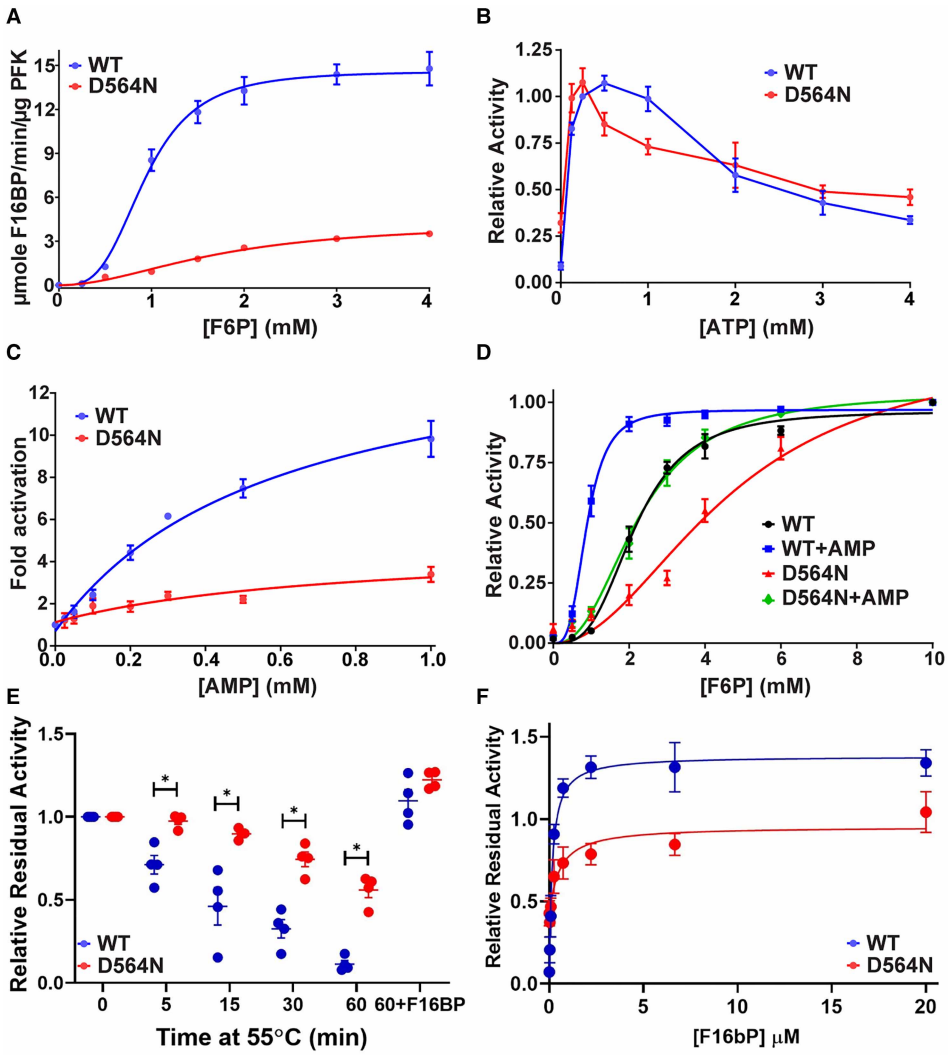

Figure 2. D564N mutation in PFKP decreases enzyme activity and alters allosteric regulation.

(**A**) Substrate affinity of PFKP (blue circles), PFKP-D564N (red circles). F6P affinity was evaluated at pH 7.5 with 0.25 mM ATP. Dots and bars represent the means ± SEM from six measurements. Lines represent a fit to the allosteric sigmoidal model. (**B**) The activation and inhibition effects of ATP on relative velocity of wild-type and mutant PFKP. The experiments were performed at 2 mM F6P and indicated ATP concentrations. Data are means ± SEM from four independent titrations. (**C**) AMP relieves the allosteric inhibition of 3 mM ATP in wild-type and to a lesser extent in the mutant protein in the presence of 2 mM F6P. Dots and bars represent the means ± SEM from three measurements. Lines represent a fit to the [agonist] versus response (three parameters) model. (**D**) 0.5 mM AMP increases substrate affinity for wild-type and mutant PFKP proteins in the presence of 1.5 mM ATP. Dots and bars represent the means ± SEM from four measurements. Lines represent a fit to the allosteric sigmoidal model. (**E**,**F**) Protection against thermal inactivation by F1,6bP. Proteins were incubated at 55°C for indicated time (**E**) or for 60 min (**F**) in the presence and absence of F1,6bP. The residual activity after incubation is expressed. * $P < 0.01$ by paired two-tailed *t*-test, $n = 3$ independent experiments.

at the interface between the catalytic and regulatory domains [8,41]. As AMP relieves ATP inhibition, we performed the assays at the inhibitory ATP concentration of 3 mM. Wild-type PFKP had a 10-fold increase in catalytic activity in response to increasing concentrations of AMP (Figure 2C), while PFKP-D564N was only activated 3-fold. We also determined how the addition of AMP effected the affinity for F6P. AMP concentration of 0.5 mM increased the affinity of wild-type PFKP 2-fold, from 2.16 ± 0.08 mM in the absence to 0.88 ± 0.03 mM in the presence of AMP (Figure 2D and Table 2). PFKP-D564N also showed an ∼2-fold increase in

Biochemical Journal (2023) **480** 1411–1427
https://doi.org/10.1042/BCJ20230207

Table 1 Saturation kinetics of wild-type and mutant PFKP and PFKL

Parameter	PFKP ($n = 6$)	PFKP-D564N ($n = 6$)	PFKL ($n = 7$)	PFKL-D553N ($n = 7$)
V_{max}^{F6P} (μM F1,6bP/min/μg)	14.62 ± 0.52	4.26 ± 0.36	9.45 ± 0.58	ND
$S_{0.5}^{F6P}$ (mM)	0.93 ± 0.05	1.73 ± 0.19	2.48 ± 0.26	ND
n_H^{F6P} (mM)	3.33 ± 0.54	1.92 ± 0.25	2.85 ± 0.70	ND

Assays were performed at pH 7.5 with 0.25 mM ATP (PFKP) or 0.125 mM ATP (PFKL). The data were fit to the allosteric sigmoidal model.
ND, not determined.

affinity for F6P, from 4.64 ± 0.68 mM to 2.25 ± 0.34 mM. These data indicate that Asp–Arg pair disruption attenuates, but does not prevent, AMP from relieving ATP inhibition. Finally, we asked if the mutation altered allosteric regulation by biphosphate sugars. F1,6bP and F2,6bP bind to an effector-binding site in the regulatory domain that is composed of residues from two protomers across the catalytic interface [15,42–45]. F1,6bP stabilizes all three human PFK1 isoforms while it only relieves ATP inhibition of PFKL and PFKM but not PFKP due to isoform-dependent coordination of F1,6bP in the allosteric sugar-binding site [25,26]. We asked if the mutation altered the ability of F1,6bP to stabilize wild-type and mutant PFKP. We focused our attention on allosteric regulation by F1,6bP as mammalian PFKP has only been co-crystallized with F1,6bP (39) and not F2,6bP. PFKP undergoes irreversible, time-dependent thermal inactivation at 55°C in the absence of ligands, with ∼10% activity remaining after 60 min of incubation (Figure 2E). PFKP-D564N lost activity at a decreased rate compared with the wild-type protein, with ∼50% activity remaining after 60 min of incubation, suggesting that PFKP-D564N has increased stability compared with the wild-type enzyme. F1,6bP protected against the loss of activity in both wild-type and mutant PFKP, both of which retained activity in the presence of 200 μM of the sugar. The mutation had no significant impact on affinity for F1,6bP, with an apparent dissociation constant of 159 nM ± 39 and 509 nM ± 310 observed for PFKP and PFKP-D564N, respectively (Figure 2F). In summary, PFKP-D564N was less active and was more resistant to thermal inactivation when compared with the wild-type protein.

We next asked if the aspartic acid to asparagine mutation had a similar effect on the activity and allosteric regulation of PFKL. The disruption of the Asp–Arg pair had a more profound effect on PFKL than on PFKP, with PFKL-D553N having almost no measurable activity under conditions that the wild-type enzyme was active (Figure 3A). We screened assay conditions to include activators and found that partial activation of the enzyme could be achieved in the presence of AMP and ammonium sulfate (Figure 3B and Table 2). Interestingly, the addition of either AMP or ammonium sulfate individually did not cause a measurable increase in PFKL-D553N activity. Therefore, the response of PFKL-D553N to allosteric effectors was measured in the presence of 5 mM ammonium sulfate and 1 mM AMP. However, as the wild-type enzyme showed no

Table 2 Effects of PFK1 activity modulators on kinetic properties of wild-type and mutant PFKP and PFKL

Metabolite	Parameter	PFKP ($n = 4$)	PFKP-D564N ($n = 4$)
1.5 mM ATP	V_{max}^{F6P}, relative	0.96 ± 0.03	1.23 ± 0.14
	$S_{0.5}^{F6P}$ (mM)	2.16 ± 0.08	4.64 ± 0.68
	n_H^{F6P} (mM)	3.11 ± 0.34	2.04 ± 0.34
1.5 mM ATP + 0.5 mM AMP	V_{max}^{F6P}, relative	0.97 ± 0.01	1.04 ± 0.04
	$S_{0.5}^{F6P}$ (mM)	0.88 ± 0.03	2.25 ± 0.11
	n_H^{F6P} (mM)	3.31 ± 0.36	2.44 ± 0.28
		PFKL ($n = 5$)	PFKL-D553N ($n = 5$)
5 mM Ammonium sulfate + 1 mM AMP	V_{max}^{F6P} (μM F1,6bP/min/μg)	ND	2.07 ± 0.13
	$S_{0.5}^{F6P}$ (mM)	ND	2.39 ± 0.27
	n_H^{F6P} (mM)	ND	1.94 ± 0.32

The kinetic parameters for PFKP and PFKL-D553N were determined at pH 7.5 with 0.25 mM ATP or 0.125 mM ATP, respectively. The parameters were generated by fitting data to the allosteric sigmoidal model.
ND, not determined.

Biochemical Journal (2023) **480** 1411–1427
https://doi.org/10.1042/BCJ20230207

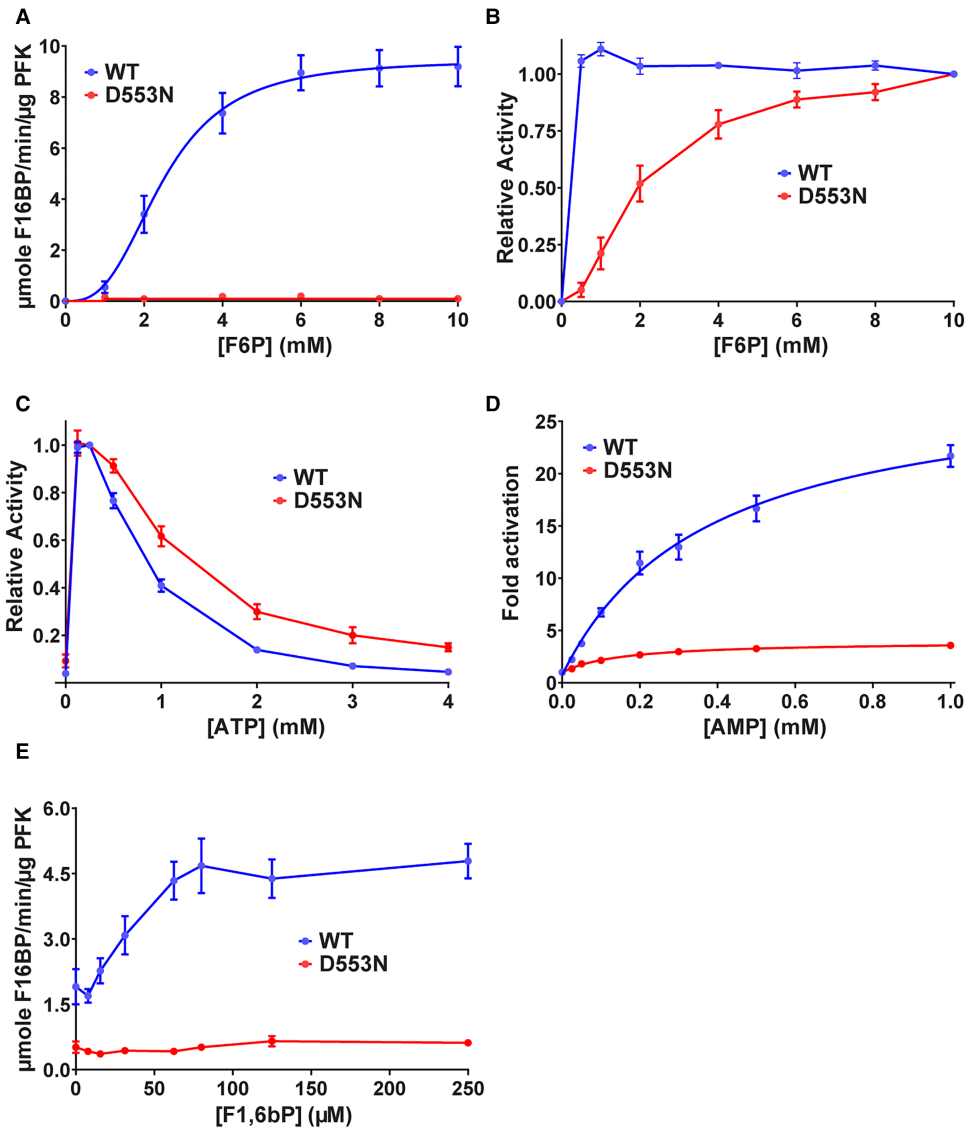

Figure 3. D553N mutation in PFKL interferes with allosteric activation by F1,6bP.

(**A**) Substrate affinity of PFKL (blue circles), PFKL-D553N (red circles). F6P affinity was evaluated at pH 7.5 with 0.125 mM ATP. Dots and bars represent the means ± SEM from seven measurements. Lines represent a fit to the allosteric sigmoidal model. (**B**) Relative activity of PFKL and PFKL-D553N in the presence of 0.125 mM ATP with 5 mM ammonium sulfate and 1 mM AMP. Data are means ± SEM from five measurements. (**C**) The activation and inhibition effects of ATP on relative velocity of wild-type and mutant PFKL. The experiments were performed at 5 mM F6P and indicated ATP concentrations. An amount of 5 mM ammonium sulfate and 1 mM AMP were added for the mutant. Data are means ± SEM from five independent titrations. (**D**) AMP relieves the allosteric inhibition of 3 mM ATP in wild-type PFKL. Activation of the mutant protein was evaluated at 0.125 mM ATP and in the presence of 5 mM ammonium sulfate. AMP titrations for both wild-type and mutant proteins were performed at 5 mM F6P. Dots and bars represent the means ± SEM from six measurements. Lines represent a fit to the [agonist] versus response (three parameters) model. (**E**) F1,6bP activates wild-type but not mutant PFKL protein in the presence of 3 mM ATP and 5 mM F6P. Dots and bars represent the means ± SEM from six measurements.

allosteric inhibition in these conditions (Figure 3B), we were only able to compare the relative regulation of the wild-type and mutant enzymes. We tested the regulation of wild-type and mutant PFKL by ATP, AMP, and F1,6bP. We found that ATP inhibited both wild-type and mutant PFKL in a similar manner, with >80% inhibition achieved by 4 mM ATP (Figure 3C). To test the ability of AMP to activate PFKL, PFKL-D553N was

Biochemical Journal (2023) **480** 1411–1427
https://doi.org/10.1042/BCJ20230207

assayed under conditions in which no ATP inhibition was observed (0.125 mM; Figure 3D) while wild-type PFKL was assayed at inhibitory ATP concentrations (3 mM). Increasing concentrations of AMP activated both wild-type and mutant PFKL (Supplemental Figure S3A). However, the relative increase in activation was higher for wild-type PFKL than for PFKL-D553N, 22-fold compared with 3.5 times, respectively. Finally, we asked if activation of PFKL by F1,6bP was altered. Wild-type PFKL showed robust activation by F1,6bP (Figure 3E). In contrast, PFKL-D553N showed no activation by F1,6bP under any of the conditions evaluated (Figure 3E and Supplemental Figure S3). Taken together, these results indicate that the aspartic acid to asparagine mutation had a more severe impact on PFKL than PFKP, decreasing enzymatic activity and attenuated the ability of F1,6bP activate the enzyme.

Structural modeling of PFKP-D564N reveal changes in electrostatic interactions

We asked if the structure of PFKP-D564N could provide insight into how disrupting the Asp–Arg pair might result in the biochemical changes observed experimentally. We determined the crystal structure of PFKP-D564N at 3.6 Å resolution (Figure 4). The atomic model had a good agreement with the crystallographic data and the expected geometric parameters (Table 3). The asymmetric unit contained one tetramer, with four protomers having essentially the same conformation. Tetrahedral anions, namely phosphate and sulfate, were bound to PFKP-D564N. Each protomer contained two phosphates; two protomers contained a phosphate bound to the allosteric sugar binding site and a prokaryotic effector site while two protomers contained both phosphates bound to prokaryotic effector sites. In contrast with previous PFKP structures, PFKP-D564N crystalized in the presence of 200 μM ammonium sulfate. We found 13 sulfate ions bound asymmetrically to the tetramer. Five sulfate residues were bound to allosteric sugar binding sites while the remaining ions were located on the surface of the tetramer. Despite the presence of ATP in the crystallization buffer, we did not observe the nucleotide bound to either the catalytic or the inhibitory binding sites. Overall, PFKP-D564N had similar structure to the wild-type enzyme (Figure 4A) with asparagine 564 found in close proximity to arginine 319. The change in amino acid identity from aspartic acid to asparagine was predicted to weaken the electrostatic interaction with guanidinium group of arginine (Figure 4B); however, it remained unclear how disrupting the Asp–Arg pair results in the changes in activity and regulation of PFKP-D564N. Thus, it is possible that the PFKP-D564N crystal lattice packing preferentially selected a certain protein conformation. To overcome this limitation, we used molecular dynamic simulations to ask how disruption of the Asp–Arg pair altered the structure of the enzyme free from crystallization constrains. We observed the backbone movements of wild-type PFKP (PDB: 4WL0) and PFKP-D564N over time and determined the root square mean deviation for wild-type (green) and mutant (blue) protein (Figure 4C). We found that wild-type PFKP had decreased movement compared with PFKP-D564N. This indicates that PFKP-D564N is further from its preferred state when locked in an active conformation in the crystal lattice and suggests that PFKP-D564N may preferentially occupy the less active t-state.

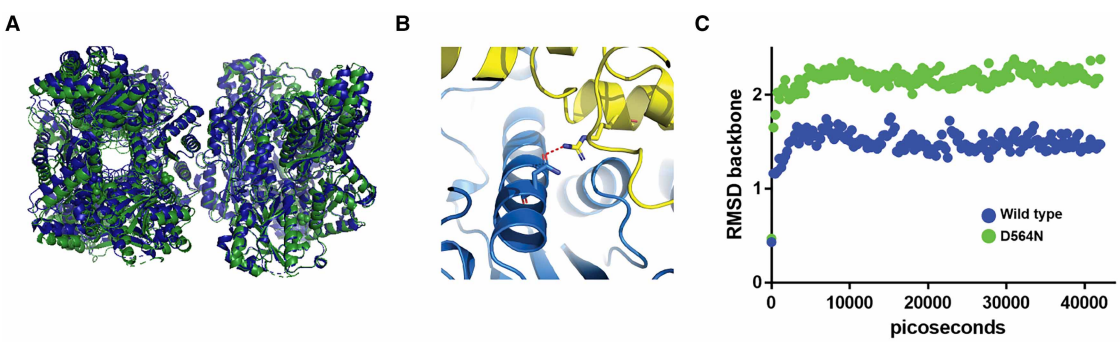

Figure 4. Crystal structure of PFKP-D564N.

(**A**) Ribbon diagram of PFKP-D564N (green) and wild-type PFKP (PDB: 4WL0, blue), showing no large structural rearrangement in the mutant protein. (**B**) High magnification view of Arg319 and Asp564. The catalytic and regulatory domains are shown in yellow and blue, respectively. Predicted electrostatic interactions are represented as red dots. (**C**) Molecular dynamic simulation of protein backbone movements for wild-type (blue) and D564N (green) PFKP.

Table 3 Data collection and refinement statistics for PFKP-D564N structure

Data collection	
Space group	$P12_11$
Cell dimensions	
a, *b*, *c* (Å)	77.89, 159.66, 131.25
α, β, γ (°)	90, 104.01, 90
Resolution (Å)	66.57–3.60 (3.73–3.60)
R_{Merge}	0.21
$I/\sigma I$	6.20
Completeness (%)	99.51 (98.90)
Redundancy	6.40
Refinement	
Resolution (Å)	3.6
No. reflections	35 995 (3602)
R_{Work}/R_{Free}	0.249/0.305
No. Atoms	22 572
Protein	22 403
Ligand/ion	105
Water	64
B-factors	
Protein	117.09
Ligand/ion	124.28
Water	89.16
R.m.s. deviations	
Bond lengths (Å)	0.001
Bond angles (°)	0.360

One crystal was used for data collection. Highest resolution shell is shown in parenthesis.

PFKP-D564N alters glycose metabolism in breast cancer cells

Finally, we asked if the expression of PFKP-D564N could alter glucose metabolism in a clinically relevant model since previous effects of the mutation were evaluated in a rat adenocarcinoma cell line expressing EGFP-labeled PFKP [15]. To address this question, FLAG-tagged wild-type PFKP and PFKP-D564N were stably expressed in the human breast cancer cell line MDA-MB-231 using a lentiviral expression system. EGFP was used as a control for viral transduction. Wild-type and mutant FLAG-PFKP were expressed at similar levels, as determined by western blot analysis (Figure 5A). The cellular rate of glycolysis, as determined by the extracellular acidification rate (ECAR) was monitored in real time using a Seahorse XF (Figure 5B). Expression of FLAG-PFKP had a minor impact on cellular glucose metabolism compared with EGFP control cells. Cells expressing FLAG-PFKP had a similar rate of basal glycolysis (Figure 5C), consistent with the high allosteric regulation of PFK1. However, a small decrease in the glycolytic capacity and glycolytic reserve (Figure 5D) was observed, suggesting that exogenous expression of FLAG-PFKP decreases the cell's maximal rate of glycolytic flux. The ratio of glycolytic activity (ECAR) to mitochondrial activity (oxygen consumption rate; OCR) was slightly decreased in FLAG-PFKP expressing cells, suggesting that expression of FLAG-PFKP rendered the cells slightly more glycolytic but did not dramatically alter the basal cellular phenotype (Figure 5E). In contrast, the expression of FLAG-PFKP-D564N displayed a dominant negative effect on cellular glycolysis in the presence of endogenous PFKP as FLAG-PFKP-D564N-expressing cells had a significant decrease in the basal rate of glycolysis when compared with either EGFP or FLAG-PFKP expressing cells. Consistent with this finding, cells

Biochemical Journal (2023) **480** 1411–1427
https://doi.org/10.1042/BCJ20230207

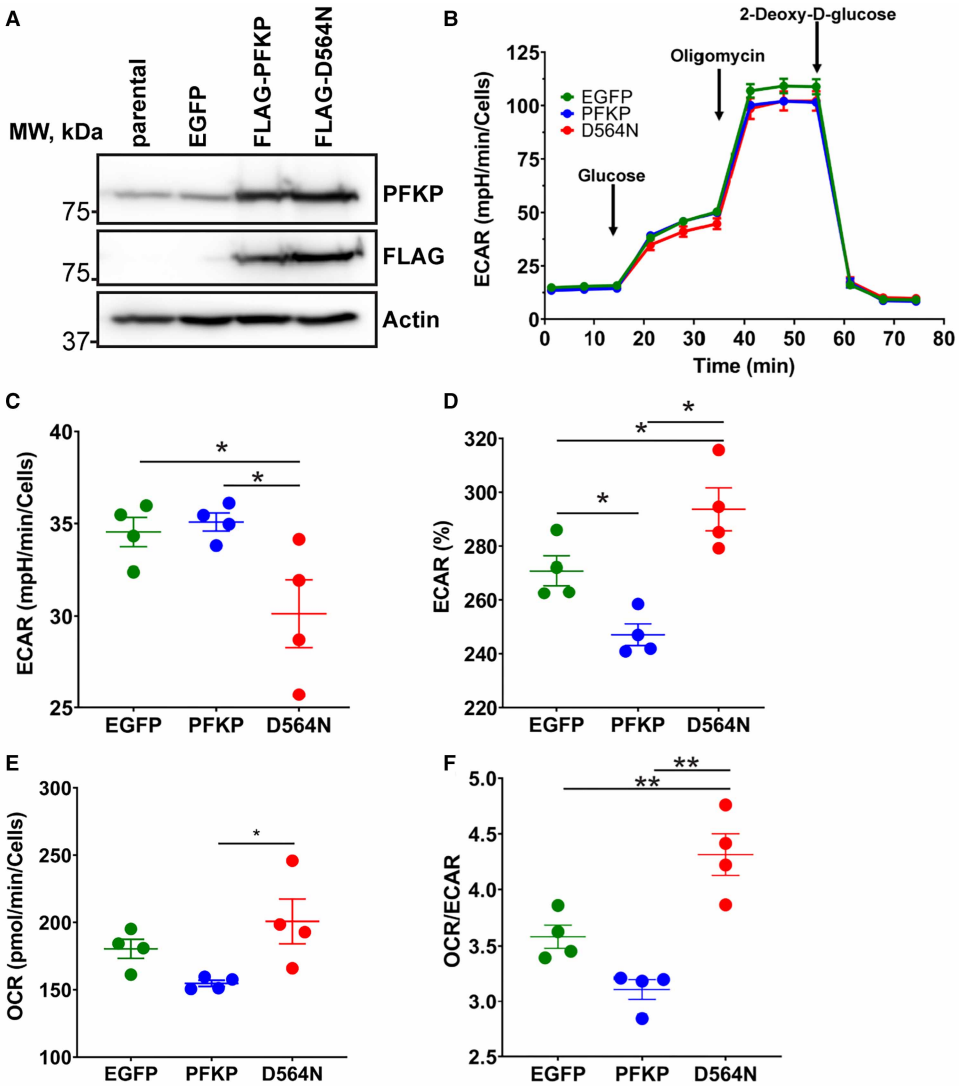

Figure 5. Human breast cancer MDA-MB-231 cells expressing PFKP-D564N have a decreased glycolysis rate.
(**A**) Representative western blot of PFKP expression in MDA-MB-231 cells. (**B**) The real-time assessment of extracellular acidification rate (ECAR) was performed by Seahorse XFe96 Analyzer, $n = 4$ independent experiments. Rate of glycolysis (**C**), percent glycolytic reserve (**D**), oxygen consumption rate (OCR) (**E**), and basal energy metabolism as defined by OCR/ECAR ratio (**F**) were determined. Data are means of four independent experiments, and error bars represent SEM. * $P < 0.05$, ** $P < 0.01$ calculated by repeated measures ANOVA followed by Tukey's multiple comparisons test.

expressing FLAG-PFKP-D564N were more reliant on mitochondrial activity than either EGFP or FLAG-PFKP expressing cells. Interestingly, the maximal glycolytic capacity of wild-type and mutant FLAG-PFKP expressing cells was the same, suggesting that low cellular energy can lead to activation of FLAG-PFKP-D564N. When oxidative phosphorylation (OXPHOS) was inhibited by oligomycin, glycolytic flux increases to generate ATP. Therefore, an increased glycolytic reserve is consistent with activation of glycolysis in FLAG-PFKP-D564N-expressing cells by signals of low cellular energy such as AMP, which was able to activate the mutant enzyme (Figure 2C).

Discussion

Here, we report a comprehensive structural and functional characterization of cancer-relevant mutations in human PFK1. Aspartic acid 564 in PFKP is located at the interface of the regulatory and catalytic domains and

forms an electrostatic bond with asparagine 319. In addition to PFKP-D564N mutation in colon cancer identified previously [15], mutations to both members of the Arg–Asp pair were also found in PFKL (Figure 1C). Asp–Arg pair located at the interface of the regulatory and catalytic domains is conserved from bacteria to humans (Figure 1D,E and Supplemental Table S1), suggesting that these residues are important for the enzyme function. Using purified recombinant proteins and enzyme kinetics we show that mutations in Asp–Arg pair decrease enzyme activity and alter allosteric regulation. Allosteric signals from effectors binding to the catalytic domain, such as ATP inhibitory signal, and from effectors binding at the catalytic and regulatory domain interface (AMP), are transmitted to the enzyme's active site. However, the activation by AMP and F1,6bP was attenuated in the Asp-to-Arg mutants compared with the wild-type enzymes. Disruption of the Asp–Arg pair had a stronger impact on PFKL compared with PFKP, possibly due to the greater allosteric regulation and decreased stability of PFKL. We determined the crystal structure of PFKP-D564N at 3.6 Å resolution to examine molecular mechanism of reduced allosteric regulation. Notably, this is the first reported structure of a human disease-associated mutation in PFK1. Molecular dynamic simulations revealed that PFKP-D564N was further from its preferred state when locked in an active conformation in the crystal lattice.

Aerobic glycolysis entails increased uptake of glucose from the environment and excretion of lactic acid regardless of oxygen availability. This metabolic program confers advantage to cancer cells by promoting fast ATP production and providing biosynthetic precursors necessary to support rapid cell proliferation [46]. Consistent with this idea, several studies demonstrated that high PFK1 expression correlates with aggressive cancer phenotype and poor patient survival [10,13]. On the other hand, context-dependent metabolic plasticity has been described throughout cancer progression and metastatic cascade [47,48]. For example, high proliferation rate of tumor cells and hypoxia inside a tumor core result in elevated oxidative stress. Cancer cells adapt to reactive oxygen species (ROS) stress by redirecting glucose catabolism from glycolysis to other pathways, such as the pentose phosphate pathway (PPP). The PPP supplies nucleotide precursors for cell proliferation and NADPH used for both ROS detoxification and catabolic metabolism [49]. Likewise, several studies demonstrated that decreased PFK1 activity in cancer switches glucose flux to the PPP, resulting in better cell viability under ROS stress [11,34,50]. Consistent with those reports, we show here that cancer-associated somatic mutations in PFK1 lower activity and alter allosteric regulation of the enzyme. We observed that breast cancer cells expressing FLAG-PFKP-D564N displayed a decreased basal rate of glycolysis compared with control cells or cells expressing wild-type FLAG-PFKP (Figure 5). These data suggest that cancer mutations reducing PFK1 activity may provide a selective advantage for cancer cell survival in tumor microenvironments where ROS stress occurs. Oxidative stress can also be caused by matrix detachment and high oxygen content in blood circulation during metastatic cascade; therefore, low PFK1 activity may promote cancer progression at multiple stages of the disease. These observations are in good agreement with those obtained for another rate-limiting glycolytic enzyme, pyruvate kinase. Cancer-associated mutations in pyruvate kinase decrease the enzyme activity and impair allosteric activation by F1,6bP, conditions that support a highly proliferative metabolic program [51]. In summary, inactivating mutations in PFK1 may contribute to malignant metabolic reprogramming to benefic adaptation to tumor microenvironment and cancer cell survival during metastatic cascade.

Understanding the molecular mechanisms of how somatic mutations alter PFK1 activity and regulation may provide insights into drug design for treating cancer, glycogen storage disease VII, and other conditions affected by altered glycolysis. The finding that a PFK1 mutation can have a dominant impact on the metabolic program of the cell may impact the way we treat Tarui disease. Individuals with Tarui disease have impaired glycolytic function, which causes the accumulation of glycogen in tissues including muscle, liver, and red blood cells. Patients with Tarui disease often display exercise intolerance, muscle weakness, cramps, and myoglobinuria [52]. Gene replacement therapy has been proposed as a potential treatment for the disease. However, this strategy requires the mutant protein does not interfere with the exogenous replacement enzyme. Therefore, knowledge of the individual mutations will be essential to predict the efficacy of these treatments. Alternatively, mutations in PFK1 which act in a dominant manner could be to targeted by small molecule pharmaceuticals to specifically activate the enzyme.

Inhibiting aerobic glycolysis by therapeutically targeting glycolytic enzymes is a current proposed strategy to limit cancer progression. Proliferative cancer cells are dependent on glucose to provide energy and biosynthetic precursors. However, this strategy is limited by the number of existing drugs, specific to a particular enzyme. Non-specific drugs, such as 2-deoxyglucose, are available but their use is limited by poor clinical outcomes due to adverse side-effects in patients. This is likely due to off-target effects due to multiple metabolic fates of glucose in the cell, such as processing through the PPP and protein glycosylation. Targeting of specific isoforms

Biochemical Journal (2023) 480 1411–1427
https://doi.org/10.1042/BCJ20230207

of glycolytic enzymes is an alternate approach that may circumvent the negative impacts of 2-deoxyglucose. However, knowledge of the identity and function of these enzymes in the cell as well as generation of specific targeting molecules will be essential for the success of this approach. Specific small molecule modulators of several glycolytic enzymes, including PFKFB3 and glucose transporters (GLUTs) inhibitors as well as pyruvate kinase isoform M2 (PKM2) activators and inhibitors, are currently being evaluated for clinical efficacy [53–59]. Until recently, there were no specific and high-affinity compounds targeting PFK1. Our studies on disruption of the Asp–Arg pair in PFK1 highlight the importance of helices 11 and 6′ in allosteric regulation and reveal that mutated amino acids on these helices contribute to dysregulated glucose metabolism in cancers and glycogen storage disease (Figure 1A) [15,39]. Residues in helices 11 and 6′ are involved in binding to allosteric effectors. For example, the allosteric activator AMP/ADP [8,41] binds to a central pocket and interacts with residues on these helices. Recently, the first non-natural agonist for PFK1, NA-11, has been reported. NA-11 interacts with residues on helices 11 and 6′, binds to the AMP/ADP effector site activating PFK1 with nM affinity [42]. Furthermore, a critical residue imparting isoform-selectivity of NA-11, lysine 315 (PFKL numbering), is located on helix 11. While there are no specific and high-affinity compounds inhibiting PFK1, the presumptive citrate-binding site includes lysine 567, located adjacent to aspartic acid 564 on helix 6′ [60]. Our findings raise the possibility of generating small molecule inhibitors of PFK1 acting to disrupt the Asp–Arg electrostatic interaction or to alter the relative orientation of helices 11 and 6′. Such compounds would be a valuable resource to determine the role of PFK1 in cancer cell metabolic reprogramming and have high potential for therapeutic use.

In summary, we used somatic mutations of PFK1 to inform our understanding of allosteric regulation by identifying key amino acid residues that are involved in the regulation of enzyme activity. Mutations to a critical Asp–Arg pair located at the catalytic-regulatory domain interface of PFK1 inhibits enzymatic activity *in vitro* and decreases glycolytic flux when expressed in cells in a dominant manner. Targeted compounds that disrupt the Asp–Arg pair may allow for highly selective therapeutic intervention to inhibit PFK1 activity.

Materials and methods

Generation and purification of recombinant PFK1

Recombinant human PFKL (NM_002626), PFKP (NM_002627.4), and the mutants were generated as described [15,20] using the Bac-to-Bac Expression system (Invitrogen) in sf9 cells. Cells were lysed in a lysis buffer (20 mM HEPES, pH 7.5; 80 mM potassium phosphate; 1 mM 2-mercaptoethanol; 10% glycerol; 10 mM imidazole, and EDTA-free Protease Inhibitor Cocktail (Abcam)) with a Dounce homogenizer. The lysates were cleared by centrifugation and the supernatants were incubated with HisPur cobalt resin (ThermoFisher Scientific). The resin was washed with lysis buffer, with high salt lysis buffer containing 1 M NaCl, and with lysis buffer again. PFK1 was eluted in lysis buffer supplemented with 100 mM imidazole. Fractions containing protein were pooled, and the buffer was exchanged for freezing buffer (20 mM 4--(2-hydroxyethyl)-1-piperazineethanesulfonic acid (HEPES) pH 7.5; 1 mM DTT; 500 μM ammonium sulfate; 5% glycerol; 1 mM ATP, and 100 μM EDTA) using a HiPrep 26/10 desalting column (GE Healthcare Life Sciences) and concentrated using an Amicon Ultracel-30K Centrifugal Filter Unit (MilliporeSigma). Protein concentration was determined using a Bradford Protein Assay kit (ThermoFisher Scientific), and aliquots snap frozen in liquid nitrogen and stored at −80°C. The quaternary structure of proteins was determined by Native-PAGE using NativePAGE Novex Bis-Tris gel system (ThermoFisher Scientific) according to the manufacturer's instructions and using Light Blue Cathode Buffer. Proteins were diluted in Native PAGE buffer (ThermoFisher Scientific) with the addition of 15 mM HEPES pH 7.5; 37.5 mM KCl; 0.75 mM DTT; and 0.9 mM ammonium sulfate. Proteins were resolved in 3–12% NativePAGE Bis-Tris gel (ThermoFisher Scientific). Proteins were identified using the Pierce Silver Stain kit (ThermoFisher Scientific) according to manufacturer's instructions.

Crystallization and structure determination

PFKP-D564N was crystallized in a buffer containing 125 μM ATP by a micro batch method at 22°C, nucleation of rod-shaped crystals occurred within four days. A solution of PFKP-D564N (5 mg/ml) was mixed in a 1 : 1 ratio with crystal solution (0.2 mM ammonium sulfate; 0.1 M Bis-Tris pH 5.5; 25% w/v Polyethylene glycol monomethyl ether 3350). Crystals were harvested and cryoprotected in 0.2 mM ammonium sulfate; 0.02 M Bis-Tris pH 5.5; 28% w/v Polyethylene glycol monomethyl ether 3350, and 30% ethylene glycol and were flash

frozen in liquid nitrogen. Data collection was performed on The Northeastern Collaborative Access Team (NE-CAT) 24-IDE beamline at The Advanced Photon Source (APS). The diffraction images were processed using XDS [61], pointless, and aimless [62–64]. The structure of ATP-bound PFKP (PDB accession number 4xyk) [15] was used to determine the structure using the molecular replacement method on Phenix Phaser-MR software [65] and structural refinement was performed with phenix.refine [66]. The data processing and refinement statistics are summarized in Table 3.

Structural analysis, alignment, and *in silico* analysis

Images highlighting the position of Arg319 and Asp564 of human PFKP (PDB file 4XYK) were generated in the PyMOL Molecular Graphics System, Version 2.0 (Schrödinger, LLC). Hydrogen bonds were predicted by the PyMOL 'Polar Contacts' command. However, the hydrogen bonds were not rigorously determined due to the low resolution of available PFK1 crystal structures. Structural alignment of *G. stearothermophilus* (PDB file 6PFK), *S. cerevisiae* (PDB file 3O8O), human PFKL (PDB file 7LW1), and human PFKP (PDB file 4XYK) was performed in PyMOL. The molecular modeling and docking studies were done using the software suit of MOE 2020.0901 (Chemical Computing Group). The protein crystal structure 4XZ2 was obtained from the Protein Data Bank (39), and prepared for downstream applications by adding hydrogens, fixing missing side chains, and adding charges at pH 7.4. Molecular dynamics simulations were done using YASARA 20.7.4 modeling suite (YASARA Biosciences GmbH) using the NOVA force field. The protein structures were mutated from D564N with the protein tools in MOE 2020.09 and minimized with the AMBER10 force field [67].

PFK1 activity assay

In vitro, PFK1 activity was determined as previously described [15,20]. Briefly, the auxiliary enzymes aldolase, triosephosphate isomerase, and glycerol phosphate dehydrogenase were purchased from MilliporeSigma, desalted using an Amicon Ultracel-10K Centrifugal Filter Unit, and resuspended in 2× Buffer containing 100 mM HEPES pH 7.5; 200 mM KCl; 2 mM DTT, and 0.3 mM NADH. The temperature was equilibrated to 25°C for 5 min before initiating the reaction with 10 mM $MgCl_2$. Absorbance at 340 nm was measured using a Varioskan LUX Multimode microplate reader (ThermoFisher Scientific). For assays containing F1,6bP, the rate of ADP production was determined using the auxiliary enzymes lactate dehydrogenase (LDH) and pyruvate kinase (MilliporeSigma) as described below. One unit of activity was defined as the amount of enzyme that catalyzed the formation of 1 μmol of fructose 1,6-bisphosphate per min. All experiments were performed with at least two separate protein preparations.

Thermal inactivation assay

The assays were performed as previously described [27] with some modifications. PFKP was diluted to 100 ng/μl in a buffer containing 50 mM HEPES pH 7.5, 100 mM KCl, 1 mM DTT and incubated at 55°C for indicated times. After incubation, the residual PFK1 activity was measured using a pyruvate kinase/LDH auxiliary enzyme plate reader assay in a buffer containing 50 mM HEPES pH 7.5, 100 mM KCl, 1 mM DTT, 0.25 mM NADH, and 0.2 mM phosphoenolpyruvic acid, 0.25 mM ATP, 5 mM F6P, and auxiliary enzymes. To determine F16bP altered PFKP stability, 200 μM F1,6bP were added to the samples before the incubation at 55°C. In experiments determining F1,6bP affinity, recombinant wild-type and mutant PFKP was diluted to 100 ng/μl in a buffer and proteins were incubated with 0–20 μM F1,6bP for 60 min at 55°C and the residual enzymatic activity measured.

Cell culture and generation of stable cell lines

MDA-MB-231 (MDA-MB-231) cells were purchased from ATCC and maintained in high-glucose DMEM (Gibco) supplemented with 10% heat-inactivated FBS (Gibco) and penicillin-streptomycin (Gibco) in 5% CO_2 at 37°C. Cells were confirmed to be mycoplasma-free by using LookOut mycoplasma detection kit (MilliporeSigma) and authenticated by STR profiling. EGFP, FLAG-PFKP, and FLAG-PFKP D564N were cloned into pLenti6.3 vector (ThermoFisher Scientific). Lentivirus particles were generated using HEK293T cells (ATCC) and ViralPower lentiviral particles packaging mix (ThermoFisher Scientific) according to the manufacturer instructions. MDA-MB-231 cells were infected with the virus particles in presence of 5 μg/ml of Polybrene (MilliporeSigma), selected with 15 μg/ml blasticidin (Gibco), and protein expression was verified by western-blotting.

Biochemical Journal (2023) **480** 1411–1427
https://doi.org/10.1042/BCJ20230207

Immunoblotting

Cells were lysed in a SDS sample buffer (63 mM Tris-hydrochloride, pH 6.8; 2% sodium dodecyl sulfate (SDS), and 10% glycerol) and protein concentration was determined using a BCA assay (ThermoFisher Scientific). An amount of 30 μg of proteins were separated by 10% polyacrylamide gel and transferred onto a polyvinylidene difluoride (PVDF) membrane (Millipore). Membranes were blocked in 5% non-fat milk in Tris Buffered Saline with 0.1% Tween-20. After the membranes were incubated with primary and secondary antibodies, immune complexes were detected using a Pierce ECL substrate (ThermoFisher Scientific) in an Amersham Imager 600 imager (GE Healthcare Life Sciences). The antibodies used in this study were against actin (Millipore, MAB1501; 1 : 5000), PFKL (Abcam, ab181064; 1 : 1000), FLAG-tag (Sigma, F1804; 1 : 1000).

Metabolic analysis of human cells

OCR and ECAR of live cells was analyzed on a Seahorse XFe96 Analyzer (Agilent Technologies). Cells were plated onto Seahorse XF96 microplate (Agilent Technologies) and allowed to attach overnight. Before assay, cells were equilibrated for 1 h in a non-CO_2 incubator at 37°C with XF DMEM base medium (Agilent Technologies) supplemented with 2 mM Glutamine (Agilent Technologies). Metabolic functions were examined through sequential injection of 10 mM glucose, 1 μM oligomycin, and 100 mM 2-deoxy-glucose (2-DG). The data were normalized by cell number measured by a CyQUANT Cell Proliferation Assay (ThermoFisher Scientific) according to the manufacturer's recommendations. Initial experiments were performed to ensure linearity of the cell number vs fluorescence intensity for each cell line. EGFP-expressing cells showed an increased baseline compared with other cell lines, due to the expression of the fluorescent protein, and cell number was quantified independently. All other cell lines showed similar results and the cell number was estimated from a single standard curve. Analysis was performed with the Agilent Seahorse Wave Desktop software.

Statistical analysis

The data represents means ± SEM. Statistical analysis was performed with GraphPad Prism software and a P-value <0.05 was considered statistically significant. At least three experiments with at least two independent protein preparations were performed to evaluate enzymatic activity.

Data reproducibility

All individual experiments described have been repeated at least three times. Initial observations of the impact of PFK1 mutations were made by Jacob Miller and Bradley Webb. These were reproduced independently and expanded upon by Maria Voronkova and Heather Hansen. Key results have been repeated independently by three experimentalists.

Data Availability

X-ray coordinates for PFKP-D564N have been deposited with the RCSB PDB databank and are accessible under the ID 7TFF.

Competing Interests

The authors declare no competing financial interests.

Funding

This work was supported by West Virginia Start-up funding to B.A.W. and A.R., Visual Sciences CoBRE project leader funding to B.A.W. (P20GM144230), and NIGMS grants to A.R. (R01GM133857) and W.J.G. (U54GM104942 and P20GM109098). This work is based upon research conducted at the Northeastern Collaborative Access Team beamlines, which are funded by the National Institute of General Medical Sciences from the National Institutes of Health (P41GM103403). The WVU Mitochondria, Metabolism & Bioenergetics Working Group, supported by the Community Foundation for the Ohio Valley Whipkey Trust.

CRediT Author Contribution

Bradley Webb: Conceptualization, Validation, Investigation, Visualization, Methodology, Writing — original draft, Project administration, Writing — review and editing. **Maria A. Voronkova:** Conceptualization, Investigation, Methodology, Writing — original draft, Writing — review and editing. **Heather L. Hansen:** Validation, Investigation, Writing — original draft, Writing — review and editing. **Madison P. Cooper:** Validation,

Investigation, Methodology. **Jacob Miller:** Conceptualization, Investigation, Methodology. **Narayanasami Sukumar:** Methodology. **Werner J. Geldenhuys:** Visualization, Methodology, Writing — review and editing. **Aaron Robart:** Visualization, Methodology, Writing — review and editing.

Acknowledgements

The authors would like to thank Mark Pinti and Morgan Glass for their excellent technical assistance. Seahorse analysis was performed by the WVU Mitochondria, Metabolism & Bioenergetics Working Group.

Abbreviations

2-DG, 2-deoxy-glucose; AMP, adenosine monophosphate; ATP, adenosine triphosphate; ECAR, extracellular acidification rate; HEPES, 4-(2-hydroxyethyl)-1-piperazineethanesulfonic acid; LDH, lactate dehydrogenase; OCR, oxygen consumption rate; PFK1, phosphofructokinase-1; PPP, pentose phosphate pathway; ROS, reactive oxygen species.

References

1 Schiliro, C. and Firestein, B.L. (2021) Mechanisms of metabolic reprogramming in cancer cells supporting enhanced growth and proliferation. *Cells* **10**, 1056 https://doi.org/10.3390/cells10051056
2 Murao, N., Yokoi, N., Takahashi, H., Hayami, T., Minami, Y. and Seino, S. (2021) Increased glycolysis affects β-cell function and identity in aging and diabetes. *Mol. Metab.* **55**, 101414 https://doi.org/10.1016/j.molmet.2021.101414
3 Goyal, M.S., Blazey, T., Metcalf, N.V., McAvoy, M.P., Strain, J.F., Rahmani, M., et al. (2023) Brain aerobic glycolysis and resilience in Alzheimer disease. *Proc. Natl Acad. Sci. U.S.A.* **120**, e2212256120 https://doi.org/10.1073/pnas.2212256120
4 Evans, P.R. and Hudson, P.J. (1979) Structure and control of phosphofructokinase from *Bacillus stearothermophilus*. *Nature* **279**, 500–504 https://doi.org/10.1038/279500a0
5 Blangy, D., Buc, H. and Monod, J. (1968) Kinetics of the allosteric interactions of phosphofructokinase from *Escherichia coli*. *J. Mol. Biol.* **31**, 13–35 https://doi.org/10.1016/0022-2836(68)90051-x
6 Poorman, R.A., Randolph, A., Kemp, R.G. and Heinrikson, R.L. (1984) Evolution of phosphofructokinase–gene duplication and creation of new effector sites. *Nature* **309**, 467–469 https://doi.org/10.1038/309467a0
7 Kemp, R.G. and Gunasekera, D. (2002) Evolution of the allosteric ligand sites of mammalian phosphofructo-1-kinase. *Biochemistry* **41**, 9426–9430 https://doi.org/10.1021/bi020110d
8 Banaszak, K., Mechin, I., Obmolova, G., Oldham, M., Chang, S.H., Ruiz, T. et al. (2011) The crystal structures of eukaryotic phosphofructokinases from baker's yeast and rabbit skeletal muscle. *J. Mol. Biol.* **407**, 284–297 https://doi.org/10.1016/j.jmb.2011.01.019
9 Schöneberg, T., Kloos, M., Brüser, A., Kirchberger, J. and Sträter, N. (2013) Structure and allosteric regulation of eukaryotic 6-phosphofructokinases. *Biol. Chem.* **394**, 977–993 https://doi.org/10.1515/hsz-2013-0130
10 Feng, Y., Zhang, Y., Cai, Y., Liu, R., Lu, M., Li, T., et al. (2020) A20 targets PFKL and glycolysis to inhibit the progression of hepatocellular carcinoma. *Cell Death Dis.* **11**, 89 https://doi.org/10.1038/s41419-020-2278-6
11 Yi, W., Clark, P.M., Mason, D.E., Keenan, M.C., Hill, C., Goddard, W.A. et al. (2012) PFK1 glycosylation is a key regulator of cancer cell growth and central metabolic pathways. *Science* **337**, 975–980 https://doi.org/10.1126/science.1222278
12 Yang, Y., Ishak Gabra, M.B., Hanse, E.A., Lowman, X.H., Tran, T.Q., Li, H., et al. (2019) MiR-135 suppresses glycolysis and promotes pancreatic cancer cell adaptation to metabolic stress by targeting phosphofructokinase-1. *Nat. Commun.* **10**, 809 https://doi.org/10.1038/s41467-019-08759-0
13 Lee, J.-H., Liu, R., Li, J., Zhang, C., Wang, Y., Cai, Q., et al. (2017) Stabilization of phosphofructokinase 1 platelet isoform by AKT promotes tumorigenesis. *Nat. Commun.* **8**, 949 https://doi.org/10.1038/s41467-017-00906-9
14 Zancan, P., Marinho-Carvalho, M.M., Faber-Barata, J., Dellias, J.M.M. and Sola-Penna, M. (2008) ATP and fructose-2,6-bisphosphate regulate skeletal muscle 6-phosphofructo-1-kinase by altering its quaternary structure. *IUBMB Life* **60**, 526–533 https://doi.org/10.1002/iub.58
15 Webb, B.A., Forouhar, F., Szu, F.-E., Seetharaman, J., Tong, L. and Barber, D.L. (2015) Structures of human phosphofructokinase-1 and atomic basis of cancer-associated mutations. *Nature* **523**, 111–114 https://doi.org/10.1038/nature14405
16 Hesterberg, L.K. and Lee, J.C. (1982) Self-association of rabbit muscle phosphofructokinase: effects of ligands. *Biochemistry* **21**, 216–222 https://doi.org/10.1021/bi00531a003
17 Costa Leite, T., Da Silva, D., Guimarães Coelho, R., Zancan, P. and Sola-Penna, M. (2007) Lactate favours the dissociation of skeletal muscle 6-phosphofructo-1-kinase tetramers down-regulating the enzyme and muscle glycolysis. *Biochem. J.* **408**, 123–130 https://doi.org/10.1042/BJ20070687
18 Dunaway, G.A. (1983) A review of animal phosphofructokinase isozymes with an emphasis on their physiological role. *Mol. Cell. Biochem.* **52**, 75–91 https://doi.org/10.1007/BF00230589
19 Dunaway, G.A., Kasten, T.P., Sebo, T. and Trapp, R. (1988) Analysis of the phosphofructokinase subunits and isoenzymes in human tissues. *Biochem. J.* **251**, 677–683 https://doi.org/10.1042/bj2510677
20 Webb, B.A., Dosey, A.M., Wittmann, T., Kollman, J.M. and Barber, D.L. (2017) The glycolytic enzyme phosphofructokinase-1 assembles into filaments. *J. Cell Biol.* **216**, 2305–2313 https://doi.org/10.1083/jcb.201701084
21 Telford, J.N., Lad, P.M. and Hammes, G.G. (1975) Electron microscope study of native and crosslinked rabbit muscle phosphofructokinase. *Proc. Natl Acad. Sci. U.S.A.* **72**, 3054–3056 https://doi.org/10.1073/pnas.72.8.3054
22 Vora, S., Seaman, C., Durham, S. and Piomelli, S. (1980) Isozymes of human phosphofructokinase: identification and subunit structural characterization of a new system. *Proc. Natl Acad. Sci. U.S.A.* **77**, 62–66 https://doi.org/10.1073/pnas.77.1.62

Biochemical Journal (2023) **480** 1411–1427
https://doi.org/10.1042/BCJ20230207

23 Fernandes, P.M., Kinkead, J.R., McNae, I.W., Michels, P.A. and Walkinshaw, M.D. (2020) Biochemical and transcript level differences between the three human phosphofructokinases show optimisation of each isoform for specific metabolic niches. *Biochem. J.* **477**, 4425–4441 https://doi.org/10.1042/BCJ20200656

24 Trivedi, B. and Danforth, W.H. (1966) Effect of pH on the kinetics of frog muscle phosphofructokinase. *J. Biol. Chem.* **241**, 4110–4112 https://doi.org/10.1016/S0021-9258(18)99819-4

25 Meienhofer, M.C., Cottreau, D., Dreyfus, J.C. and Kahn, A. (1980) Kinetic properties of human F4 phosphofructokinase: a poor regulatory enzyme. *FEBS Lett.* **110**, 219–222 https://doi.org/10.1016/0014-5793(80)80077-9

26 Tornheim, K. (1985) Activation of muscle phosphofructokinase by fructose 2,6-bisphosphate and fructose 1,6-bisphosphate is differently affected by other regulatory metabolites. *J. Biol. Chem.* **260**, 7985–7989 https://doi.org/10.1016/S0021-9258(17)39551-0

27 Sánchez-Martínez, C., Estévez, A.M. and Aragón, J.J. (2000) Phosphofructokinase C isozyme from ascites tumor cells: cloning, expression, and properties. *Biochem. Biophys. Res. Commun.* **271**, 635–640 https://doi.org/10.1006/bbrc.2000.2681

28 Tarui, S., Okuno, G., Ikura, Y., Tanaka, T., Suda, M. and Nishikawa, M. (1965) Phosphofructokinase deficiency in skeletal muscle. a new type of glycogenosis. *Biochem. Biophys. Res. Commun.* **19**, 517–523 https://doi.org/10.1016/0006-291x(65)90156-7

29 Raben, N. and Sherman, J.B. (1995) Mutations in muscle phosphofructokinase gene. *Hum. Mutat.* **6**, 1–6 https://doi.org/10.1002/humu.1380060102

30 Warburg, O. (1956) On the origin of cancer cells. *Science* **123**, 309–314 https://doi.org/10.1126/science.123.3191.309

31 Vander Heiden, M.G., Cantley, L.C. and Thompson, C.B. (2009) Understanding the Warburg effect: the metabolic requirements of cell proliferation. *Science* **324**, 1029–1033 https://doi.org/10.1126/science.1160809

32 Moreno-Sánchez, R., Marín-Hernández, A., Gallardo-Pérez, J.C., Quezada, H., Encalada, R., Rodríguez-Enríquez, S. et al. (2012) Phosphofructokinase type 1 kinetics, isoform expression, and gene polymorphisms in cancer cells. *J. Cell. Biochem.* **113**, 1692–1703 https://doi.org/10.1002/jcb.24039

33 Zancan, P., Sola-Penna, M., Furtado, C.M. and Da Silva, D. (2010) Differential expression of phosphofructokinase-1 isoforms correlates with the glycolytic efficiency of breast cancer cells. *Mol. Genet. Metab.* **100**, 372–378 https://doi.org/10.1016/j.ymgme.2010.04.006

34 Kim, N.H., Cha, Y.H., Lee, J., Lee, S.-H., Yang, J.H., Yun, J.S., et al. (2017) Snail reprograms glucose metabolism by repressing phosphofructokinase PFKP allowing cancer cell survival under metabolic stress. *Nat. Commun.* **8**, 14374 https://doi.org/10.1038/ncomms14374

35 DeBerardinis, R.J. and Chandel, N.S. (2016) Fundamentals of cancer metabolism. *Sci. Adv.* **2**, e1600200 https://doi.org/10.1126/sciadv.1600200

36 Lu, J., Tan, M. and Cai, Q. (2015) The Warburg effect in tumor progression: mitochondrial oxidative metabolism as an anti-metastasis mechanism. *Cancer Lett.* **356**, 156–164 https://doi.org/10.1016/j.canlet.2014.04.001

37 Park, J.S., Burckhardt, C.J., Lazcano, R., Solis, L.M., Isogai, T., Li, L., et al. (2020) Mechanical regulation of glycolysis via cytoskeleton architecture. *Nature* **578**, 621–626 https://doi.org/10.1038/s41586-020-1998-1

38 Shirakihara, Y. and Evans, P.R. (1988) Crystal structure of the complex of phosphofructokinase from *Escherichia coli* with its reaction products. *J. Mol. Biol.* **204**, 973–994 https://doi.org/10.1016/0022-2836(88)90056-3

39 Vives-Corrons, J.-L., Koralkova, P., Grau, J.M., Mañú Pereira, M.D.M. and Van Wijk, R. (2013) First description of phosphofructokinase deficiency in Spain: identification of a novel homozygous missense mutation in the PFKM gene. *Front. Physiol.* **4**, 393 https://doi.org/10.3389/fphys.2013.00393

40 Brüser, A., Kirchberger, J. and Schöneberg, T. (2012) Altered allosteric regulation of muscle 6-phosphofructokinase causes Tarui disease. *Biochem. Biophys. Res. Commun.* **427**, 133–137 https://doi.org/10.1016/j.bbrc.2012.09.024

41 Brüser, A., Kirchberger, J., Kloos, M., Sträter, N. and Schöneberg, T. (2012) Functional linkage of adenine nucleotide binding sites in mammalian muscle 6-phosphofructokinase. *J. Biol. Chem.* **287**, 17546–17553 https://doi.org/10.1074/jbc.M112.347153

42 Amara, N., Cooper, M.P., Voronkova, M.A., Webb, B.A., Lynch, E.M., Kollman, J.M., et al. (2021) Selective activation of PFKL suppresses the phagocytic oxidative burst. *Cell* **184**, 4480–4494.e15 https://doi.org/10.1016/j.cell.2021.07.004

43 Kloos, M., Brüser, A., Kirchberger, J., Schöneberg, T. and Sträter, N. (2015) Crystal structure of human platelet phosphofructokinase-1 locked in an activated conformation. *Biochem. J* **469**, 421–432 https://doi.org/10.1042/BJ20150251

44 Tornheim, K. and Lowenstein, J.M. (1976) Control of phosphofructokinase from rat skeletal muscle. Effects of fructose diphosphate, AMP, ATP, and citrate. *J. Biol. Chem.* **251**, 7322–7328 https://doi.org/10.1016/S0021-9258(17)32852-1

45 Uyeda, K., Furuya, E. and Luby, L.J. (1981) The effect of natural and synthetic D-fructose 2,6-bisphosphate on the regulatory kinetic properties of liver and muscle phosphofructokinases. *J. Biol. Chem.* **256**, 8394–8399 https://doi.org/10.1016/S0021-9258(19)68856-3

46 Pavlova, N.N. and Thompson, C.B. (2016) The emerging hallmarks of cancer metabolism. *Cell Metab.* **23**, 27–47 https://doi.org/10.1016/j.cmet.2015.12.006

47 Faubert, B., Solmonson, A. and DeBerardinis, R.J. (2020) Metabolic reprogramming and cancer progression. *Science* **368**, eaaw5473 https://doi.org/10.1126/science.aaw5473

48 Kreuzaler, P., Panina, Y., Segal, J. and Yuneva, M. (2020) Adapt and conquer: metabolic flexibility in cancer growth, invasion and evasion. *Mol. Metab.* **33**, 83–101 https://doi.org/10.1016/j.molmet.2019.08.021

49 Tong, X., Zhao, F. and Thompson, C.B. (2009) The molecular determinants of de novo nucleotide biosynthesis in cancer cells. *Curr. Opin. Genet. Dev* **19**, 32–37 https://doi.org/10.1016/j.gde.2009.01.002

50 Kobayashi, H., Hatakeyama, H., Nishimura, H., Yokota, M., Suzuki, S., Tomabechi, Y., et al. (2021) Chemical reversal of abnormalities in cells carrying mitochondrial DNA mutations. *Nat. Chem. Biol.* **17**, 335–343 https://doi.org/10.1038/s41589-020-00676-4

51 Liu, V.M., Howell, A.J., Hosios, A.M., Li, Z., Israelsen, W.J. and Vander Heiden, M.G. (2020) Cancer-associated mutations in human pyruvate kinase M2 impair enzyme activity. *FEBS Lett.* **594**, 646–664 https://doi.org/10.1002/1873-3468.13648

52 Tarui, S., Kono, N. and Uyeda, K. (1972) Purification and properties of rabbit erythrocyte phosphofructokinase. *J. Biol. Chem.* **247**, 1138–1145 https://doi.org/10.1016/S0021-9258(19)45625-1

53 Jiang, J., Walsh, M.J., Brimacombe, K.R., Anastasiou, D., Yu, Y., Israelsen, W.J. et al. (2010) ML265: A potent PKM2 activator induces tetramerization and reduces tumor formation and size in a mouse xenograft model. In *Probe Reports From the NIH Molecular Libraries Program*, National Center for Biotechnology Information (US), Bethesda, MD Accessed August 2, 2021. http://www.ncbi.nlm.nih.gov/books/NBK153222/

54 Vander Heiden, M.G., Christofk, H.R., Schuman, E., Subtelny, A.O., Sharfi, H., Harlow, E.E. et al. (2010) Identification of small molecule inhibitors of pyruvate kinase M2. *Biochem. Pharmacol.* **79**, 1118–1124 https://doi.org/10.1016/j.bcp.2009.12.003

55 Shriwas, P., Chen, X., Kinghorn, A.D. and Ren, Y. (2020) Plant-derived glucose transport inhibitors with potential antitumor activity. *Phytother. Res.* **34**, 1027–1040 https://doi.org/10.1002/ptr.6587
56 Chan, D.A., Sutphin, P.D., Nguyen, P., Turcotte, S., Lai, E.W., Banh, A., et al. (2011) Targeting GLUT1 and the Warburg effect in renal cell carcinoma by chemical synthetic lethality. *Sci. Transl. Med.* **3**, 94ra70 https://doi.org/10.1126/scitranslmed.3002394
57 Clem, B., Telang, S., Clem, A., Yalcin, A., Meier, J., Simmons, A., et al. (2008) Small-molecule inhibition of 6-phosphofructo-2-kinase activity suppresses glycolytic flux and tumor growth. *Mol. Cancer Ther.* **7**, 110–120 https://doi.org/10.1158/1535-7163.MCT-07-0482
58 Clem, B.F., O'Neal, J., Tapolsky, G., Clem, A.L., Imbert-Fernandez, Y., Kerr, D.A., et al. (2013) Targeting 6-phosphofructo-2-kinase (PFKFB3) as a therapeutic strategy against cancer. *Mol. Cancer Ther.* **12**, 1461–1470 https://doi.org/10.1158/1535-7163.MCT-13-0097
59 Liu, Y., Cao, Y., Zhang, W., Bergmeier, S., Qian, Y., Akbar, H., et al. (2012) A small-molecule inhibitor of glucose transporter 1 downregulates glycolysis, induces cell-cycle arrest, and inhibits cancer cell growth *in vitro* and *in vivo*. *Mol. Cancer Ther.* **11**, 1672–1682 https://doi.org/10.1158/1535-7163.MCT-12-0131
60 Li, Y., Rivera, D., Ru, W., Gunasekera, D. and Kemp, R.G. (1999) Identification of allosteric sites in rabbit phosphofructo-1-kinase. *Biochemistry* **38**, 16407–16412 https://doi.org/10.1021/bi991761l
61 Kabsch, W. (2010) Integration, scaling, space-group assignment and post-refinement. *Acta Crystallogr. D Biol. Crystallogr.* **66**, 133–144 https://doi.org/10.1107/S0907444909047374
62 Evans, P.R. (2011) An introduction to data reduction: space-group determination, scaling and intensity statistics. *Acta Crystallogr. D Biol. Crystallogr.* **67**, 282–292 https://doi.org/10.1107/S090744491003982X
63 Evans, P.R. and Murshudov, G.N. (2013) How good are my data and what is the resolution? *Acta Crystallogr. D Biol. Crystallogr.* **69**, 1204–1214 https://doi.org/10.1107/S0907444913000061
64 Evans, P. (2006) Scaling and assessment of data quality. *Acta Crystallogr. D Biol. Crystallogr.* **62**, 72–82 https://doi.org/10.1107/S0907444905036693
65 McCoy, A.J., Grosse-Kunstleve, R.W., Adams, P.D., Winn, M.D., Storoni, L.C. and Read, R.J. (2007) Phaser crystallographic software. *J. Appl. Crystallogr.* **40**, 658–674 https://doi.org/10.1107/S0021889807021206
66 Liebschner, D., Afonine, P.V., Baker, M.L., Bunkóczi, G., Chen, V.B., Croll, T.I., et al. (2019) Macromolecular structure determination using X-rays, neutrons and electrons: recent developments in Phenix. *Acta Crystallogr. D Struct. Biol.* **75**, 861–877 https://doi.org/10.1107/S2059798319011471
67 Case, D.A., Cheatham, T.E., Darden, T., Gohlke, H., Luo, R., Merz, K.M. et al. (2005) The Amber biomolecular simulation programs. *J. Comput. Chem.* **26**, 1668–1688 https://doi.org/10.1002/jcc.20290
68 Tate, J.G., Bamford, S., Jubb, H.C., Sondka, Z., Beare, D.M., Bindal, N., et al. (2019) COSMIC: the catalogue of somatic mutations in cancer. *Nucleic Acids Res.* **47**, D941–D947 https://doi.org/10.1093/nar/gky1015